J. Water Environ. Nanotechnol., 8(3): 215-228 Summer 2023

ORIGINAL RESEARCH PAPER

Photocatalytic Dynamic Membrane Containing Graphitic Carbon Nitride/Zirconium dioxide Nanocomposite for MB and CR Dye Removal under Household LED Lamp

Marjan Tanzifi[*,1], Mohsen Jahanshahi[1,2], Majid Peyravi[1], Soodabeh Khalili[1,2]*

[1] Department of Chemical Engineering, Babol Noshirvani University of Technology, Babol, Iran
[2] Nanotechnology Research Institute, Babol Noshirvani University of Technology, Babol, Iran

Received: 2023-04-22 Accepted: 2023-05-11 Published: 2023-08-09

ABSTRACT

Dye-containing wastewater is a major pollutant that can irreversibly damage the environment. Ultrafiltration membrane technology combined with photocatalysis is used for the treatment of dye-containing solutions. To remove dye pollution, Methylene blue (MB) and Congo red (CR), graphitic carbon nitride (CNG), and its zirconium dioxide nanocomposite (CNGZ) were used in the photocatalytic dynamic membrane system in both self-forming and pre-coated modes under household LED light. The filtration results of the self-forming membrane showed that the pure CNG- and nanocomposite-based photocatalytic membrane systems were more efficient for MB and CR dye removal than the photocatalytic system in batch mode. In addition to improving dye molecule removal efficiency, adding the photocatalyst to the PES membrane also significantly increased water flux. Moreover, the respective MB and CR rejection rates were 29% and 47% for the pure PES membrane and 89% in 120 min, and 100% in 80 min for the CNGZ-based photocatalytic membrane. This suggests that the photocatalytic membrane system is a more effective dye pollution remover than the pure PES. For comparison, the pre-coated dynamic membrane system used for MB dye removal was good for removing 98.6% within 20 min. The results suggest that CNGZ-based photocatalytic dynamic membrane is a promising technology for increasing dye molecules removal efficiency and flux in the remediation of dye-containing wastewater.

Keywords: Dynamic membrane, Photocatalysis, Decolorization, Graphitic carbon nitride, Household LED irradiation.

How to cite this article

Tanzifi M., Jahanshahi M., Peyravi M., Khalili S., Photocatalytic Dynamic Membrane Containing Graphitic Carbon Nitride/Zirconium dioxide Nanocomposite for MB and CR Dye Removal under Household LED Lamp. J. Water Environ. Nanotechnol., 2023; 8(3): 215-228. DOI: 10.22090/jwent.2023.03.002

INTRODUCTION

The organic dyes released into water and wastewater by various industries have prompted widespread environmental concerns worldwide. The unchecked discharge of dye-containing wastewater into the environment damages human health, causes disease, and endangers the aquatic ecosystem, plants, and animals [1-3]. In the event of contact, dye pollutants permanently damage the eyes and irritate the skin [4]. They are carcinogenic and will cause burning mouth syndrome, dizziness, heavy sweating, nausea, and methemoglobinemia [5,6]. Dye-containing wastewater increases water turbidity after entering natural water sources, preventing light, which is essential for the synthesis and respiration of aquatic organisms, from entering water [7,8]. Therefore, these toxic and dangerous pollutants must be removed from wastewater before release into the environment.

Membrane filtration is an integral and continuous stage in advanced wastewater treatment, including dye-containing wastewater. It consists of microfiltration, ultrafiltration, nanofiltration, and reverse osmosis. The numerous advantages of these pressure-driven physical methods include

* Corresponding Authors Email: *ma_tanzifi@yahoo.com*

the production of clean water, good efficiency, easy operation, lack of chemicals, and feasibility of large-scale production [9,10]. Although nanofiltration removes dye molecules at a high rejection rate with its particle size-based separation mechanism, it has disadvantages such as low water flux, fouling, and high energy consumption. Meanwhile, despite its higher water flux, the wider pores in ultrafiltration can allow some dye molecules to pass through, resulting in a lower rejection rate than nanofiltration [11,12]. Ultrafiltration is also constrained by the residual pollutant molecules in the feed solution, which should be removed in some way [13,14]. To address these constraints, ultrafiltration can be combined with advanced oxidation processes such as photocatalysis to create a photocatalytic membrane system with greater pollutant removal efficiency [2, 15-17]. Photocatalysis is an advanced oxidation technology in which photocatalyst material is excited to produce free radicals to degrade pollutant molecules under irradiation [18-21]. The photocatalytic membrane system addresses the problem of photocatalyst particle recovery from the solution, reduces membrane fouling by photocatalysis, and increases flux. Thus, the individual limitations of photocatalysis and membrane filtration are both addressed [22-24].

Photocatalytic dynamic membranes can be self-forming or pre-coated. The former initially mix wastewater with the photocatalyst and filter using the support membrane; whereas the latter put photocatalyst particles under pressure on the support membrane before wastewater filtration [2,25]. Habibollahi et al. [2] synthesized and used the Ag-ZnO/g-C_3N_4/GO nanocomposite photocatalyst in the photocatalytic dynamic membrane (self-forming and pre-coated) to remove methylene blue dye. The results showed that the synthesized photocatalyst improved the rejection rate, flux, and the hydrophilicity of membrane surface in the photocatalytic membrane system. Compared to the static mode, the photocatalytic dynamic membrane also provided better and faster dye degradation. Liu et al. [22] used the dead-end filtration system to deposit different amounts of the $ZnIn_2S_4$ photocatalyst on the PVDF membrane, fabricating a pre-coated photocatalytic dynamic membrane. The results illustrated that with 2.6 mg/cm^2 of photocatalyst loading, the photocatalytic dynamic membrane was more efficient for Fluvastatin (97.19%) and TOC (53.29%) removal than pure PVDF. Gao et al. [26] employed a photocatalytic dynamic membrane with the $ZnIn_2S_4$ photocatalyst for removing tetracycline. The results suggested that the dynamic $ZnIn_2S_4$ layer led to 57% tetracycline mineralization after 3 hr of filtration. Also, 92% tetracycline (100 $\frac{\mu g}{L}$) removal efficiency was retained during 36 hr of reaction.

Numerous water and wastewater treatment researchers have developed an interest in medium-band-gap photocatalyst material (active in the visible light spectrum). This can be attributed to the high percentage of visible light (45%) in sunlight, which is merely 7% for UV light. Therefore, photocatalysts capable of photocatalytic activity under sunlight are preferable [27-31]. Two-dimensional graphitic carbon nitride is a non-toxic semiconductor with easy synthesis and an average bandgap energy of about 2.7 eV. Hence, it provides adequate photocatalytic activity under visible light and is capable of photodegrading organic pollutants through oxidation-reduction (redox) reactions. To increase its photocatalytic activity and delay the recombination of electron-hole pairs, this semiconductor can be combined with another semiconductor with a larger band gap and conduction and valence band energies that closely emulate the conduction and valence band energies of graphitic carbon nitride to prepare the graphitic carbon nitride/semiconductor nanocomposite [32,33]. Despite studies on using graphitic carbon nitride and its composites for making photocatalytic membranes, it has limited use for producing photocatalytic dynamic membranes and removing dye pollutants. Therefore, this study aimed to use the graphitic carbon nitride/zirconium dioxide nanocomposite to fabricate a self-forming and pre-coated photocatalytic dynamic membrane and use it for the treatment of dye-contaminated wastewater (MB and CR solutions) under LED light exposure. The pure membrane and the photocatalytic dynamic membrane will be compared in terms of rejection rate and permeation flux in removing MB and CR dyes. Moreover, the photocatalytic membrane will be compared with the batch photocatalytic system in terms of dye removal efficiency under LED irradiation. To fit the experimental data with kinetic models, the zero-, first- and second-order models were used in batch photocatalytic systems and self-forming photocatalytic dynamic membranes to comprehend the system kinetics.

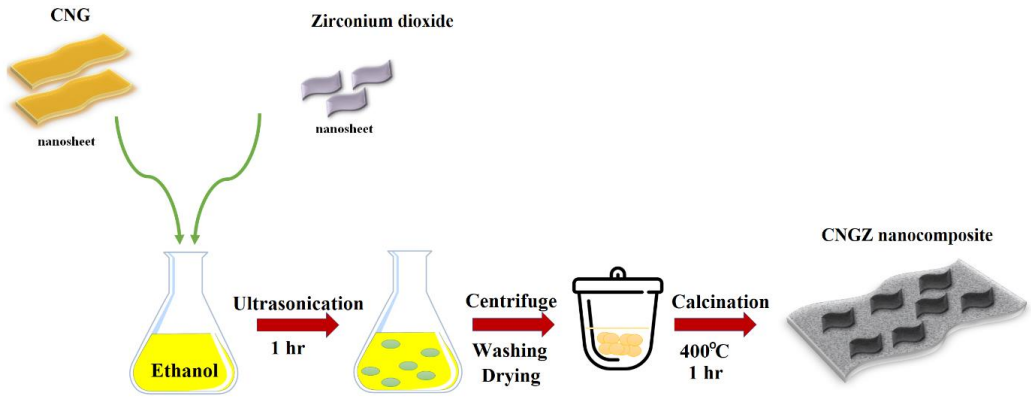

Scheme 1. Schematic illustration for the synthesis of CNGZ nanocomposite.

EXPERIMENTAL

Materials

This part was presented in SI, section 1.

Synthesis of Graphitic carbon nitride/Zirconium dioxide nanocomposite

The synthesis of pure graphitic carbon nitride and pure zirconium dioxide is explained in our previous study [34]. To summarize the nanocomposite synthesis, graphitic carbon nitride, and zirconium dioxide nanosheets with an equal mass ratio were added to a specific amount of ethanol, dispersed in an ultrasonic bath for 1 hr, and finally stirred on a magnetic stirrer for 20 hr. The final mixture was oven-dried after centrifugation and multiple washes with water and ethanol. To link the two photocatalysts' nanosheets, the resultant powder was calcined in a tube furnace at 400°C for 1 hr (Scheme 1). The graphitic carbon nitride was abbreviated as CNG and the resultant nanocomposite was called CNGZ.

Preparation of polyethersulfone membrane

The polyethersulfone (PES) membrane was synthesized through a phase inversion process based on the method proposed in our previous study [2]. To synthesize a 16 wt% membrane, PES was added to the DMF (dimethylformamide) solvent and stirred slowly at room temperature for 12 hr until obtaining a fully transparent solution. After remaining steady for 6 hr for degassing, the polymer solution was slowly poured on a piece of polyester glued on glass, where it was spread and molded using a casting knife. Then, to form a solid membrane through phase inversion, the membrane was immediately placed in a distilled water bath. To ensure complete phase inversion and removal of the impurities and residual solvent, the membrane was left in a water bath for 24 hr before it was removed and put between two pieces of filter paper to dry completely.

Batch photocatalytic system

To examine the MB and CR dye degradation capacity of the synthesized photocatalysts, a specific amount of the photocatalyst was added to 100 ml of the dye solution with a concentration of 10 $\frac{mg}{L}$ and stirred. Before light irradiance, the mixture was stirred for 30 min in the dark to reach adsorption-desorption equilibrium between the photocatalyst and the pollutant molecules. Then, the photocatalytic reaction was completed under a 100 W household LED lightbulb (with a UV light filter) as the visible light source. During dye degradation, a specific amount of the dye solution was extracted within 20 min and its concentration was measured using the spectrophotometer (in maximum wavelengths of 668 nm and 496 nm for the MB and CR dyes, respectively). The dye removal efficiency was calculated using the following equation:

$$R(\%) = \frac{C_i - C_t}{C_i} \times 100 \quad (1)$$

Where, C_i and C_t denote the initial dye concentration and dye concentration at time *t*, respectively.

Self-forming photocatalytic dynamic filtration

First, the synthesized PES membrane was cut down to specific dimensions and placed inside a plexiglass cell with 15.2 cm^2 of area and 150 ml of volume in a dead-end system. Then, a

specific amount of the synthesized photocatalyst was mixed with 150 ml of 10 $\frac{mg}{L}$ dye solution and poured into the cell and the system was put under 1 bar of nitrogen gas pressure. To activate the photocatalyst, the membrane setup was put under a 100 W household LED lamp. An output sample was taken every 20 min for concentration measurement. Dye molecule rejection rate and permeation flux were respectively obtained using equations 2 and 3:

$$R(\%) = \frac{C_f - C_p}{C_f} \times 100 \quad (2)$$

$$F = \frac{V}{A \times t} \quad (3)$$

Where, C_f and C_p represent dye concentration in feed and permeate solutions, respectively. Also, V, A, and t are the volume of collected permeation (L), effective filtration area (m^2) and filtration time (hr), respectively.

Pre-coated photocatalytic dynamic filtration

At first, a specific amount of photocatalyst was added to a specific volume of distilled water, which is then stirred for a certain period. Then, the resultant solution was poured into the dead-end membrane system containing a piece of PES membrane at the end and applies pressure via nitrogen gas to remove all distilled water from the system output and create a layer of the photocatalyst on the PES membrane surface. After layer formation, the 150 mL dye solution with 10 ppm of concentration was added to the system. The system was put under 1 bar of nitrogen gas pressure in the presence of a household LED light for a specified time. Note that permeation concentration and volume were measured at 20-min intervals.

Kinetic Study

Zero-, first- and second-order kinetic models were used for investigating the degradation kinetics of MB and CR dyes in the batch system and the self-forming photocatalytic dynamic membrane using the following equations [2,35]:

$$C_0 - C_t = k_0 t \quad (4)$$

$$Ln\left(\frac{C_0}{C_t}\right) = k_1 t \quad (5)$$

$$\frac{1}{C_t} - \frac{1}{C_0} = k_2 t \quad (6)$$

Where, C_0 and C_t are the initial (t=0) and secondary dye concentrations (t=t), (mg/L), respectively. Also, $k_0\left(\frac{mg}{L.min}\right)$, $k_1\left(\frac{1}{min}\right)$ and $k_2\left(\frac{L}{mg.min}\right)$ are the rate constants of the zero-, first- and second-order kinetic models, respectively.

RESULTS AND DISCUSSION

TEM, FESEM, PL, and XPS analysis

Fig. 1 shows the morphology and particle size of the CNG photocatalyst and its nanocomposite with zirconium dioxide using TEM analysis. Fig. 1a shows that pure zirconium dioxide has a thin, transparent, and planar structure with a length of several hundred nanometers. However, CNG has much larger transparent sheets exceeding 1 μm in length (Fig. 1b). Figs.1c and d illustrate that zirconium dioxide fits well in the CNG structure with adequate proximity and overlap. The proper integration of the two materials' nanostructures leads to a high electron transfer rate between materials, reducing electron-hole pair recombination and PL intensity (Fig. 1e) and increasing the photocatalytic activity of the nanocomposite [36]. According to the results of DRS (SI, section 2), the band gap energies of CNG, CNGZ nanocomposite, and zirconium dioxide are 2.76 eV, 2.67 eV, and 4.01 eV, respectively, indicating the visible-light-driven photocatalytic performance of CNG and CNGZ, and UV-driven photocatalytic performance of zirconium dioxide.

Moreover, Fig. 1f shows the FESEM image of the support membrane surface (PES). The support membrane has smaller pores than the nanocomposite photocatalyst structure (SI, section 3), suggesting that in the pre-coated mode, the photocatalyst tends to be deposited on the membrane surface than within its pores. The photocatalyst particles placed on the PES membrane surface prevent pollutants from

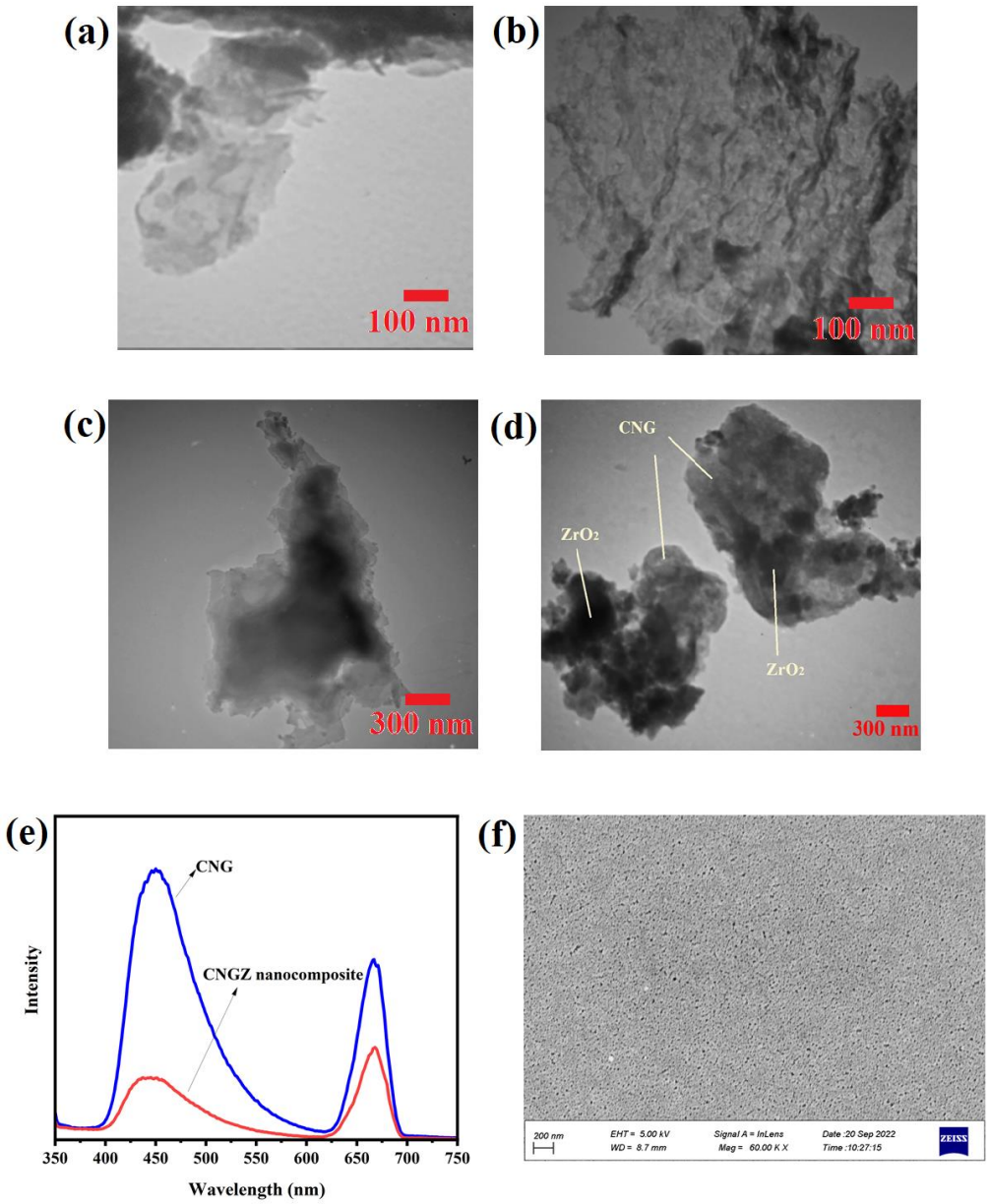

Fig. 1. TEM image of (a) pure zirconium dioxide (b) CNG and (c,d) CNGZ nanocomposite. (e) PL spectra of CNG and CNGZ, (f) surface FESEM image of PES membrane.

contacting the support membrane surface and permeating into membrane pores.

Data about the elemental composition and graphitic carbon nitride and zirconium dioxide bonds were obtained using XPS analysis and results are presented in Fig. 2. Fig. 2a illustrates the XPS spectra (full scan) of the pure CNG and CNGZ nanocomposite. The N and C elements are observed in CNG-associated spectra, while the XPS spectra of the CNGZ nanocomposite show Zr, O, N, and C elements, which are related to the presence of both semiconductors in the nanocomposite structure [37,38]. Also, the high-resolution spectra of elements (C 1s and N 1s) are presented in Figs. 2b and c, respectively. According to Fig. 2b, CNG-associated C 1s spectra display two peaks at 284.6 and 288.1 eV, which are related to the sp^2 C-C and sp^3 N=C-N binding energies, respectively. It is noteworthy, the new diffraction peak at 286.7 eV (in the CNGZ-associated C 1s spectra) corresponds

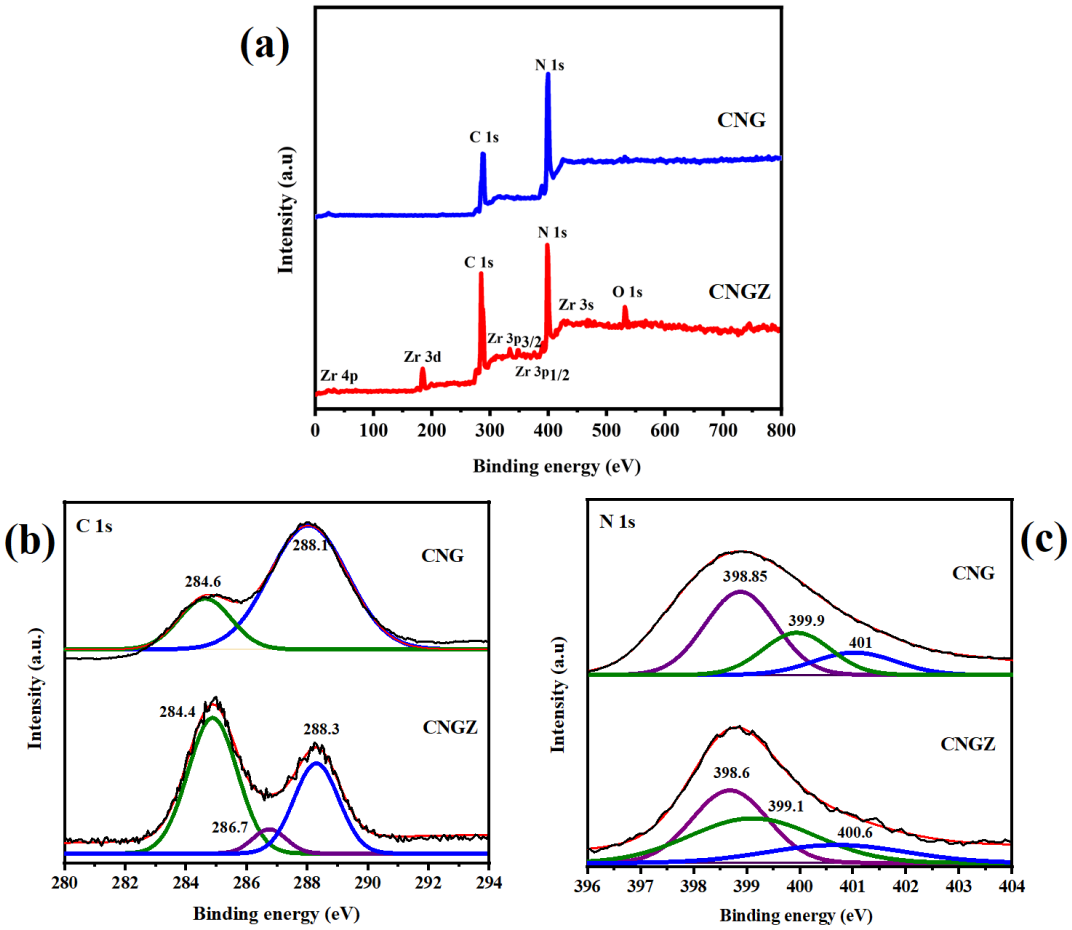

Fig. 2. XPS spectra of the CNG and CNGZ nanocomposite: (a) full scan spectrum, (b) C 1 s, and (c) N 1 s.

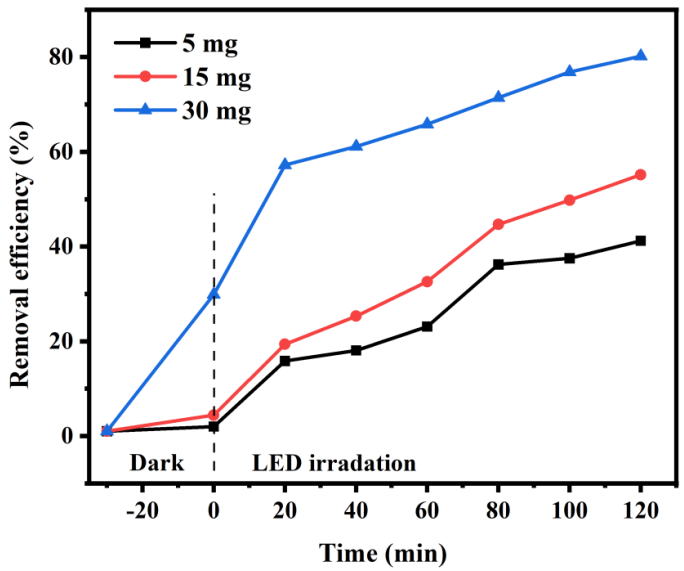

Fig. 3. Effect of CNGZ nanocomposite dose on the degradation efficiency of MB dye (dye concentration: 10 mg/L, volume: 100 ml).

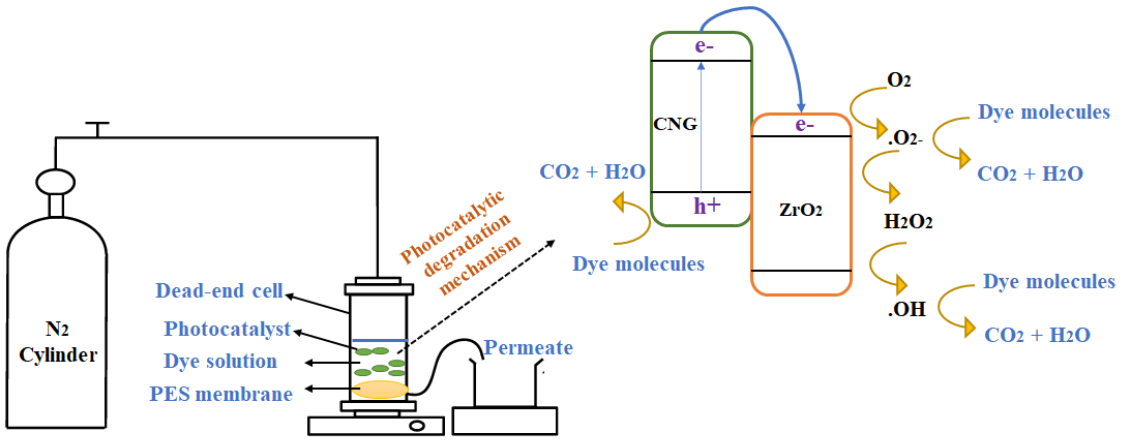

Scheme 2. A possible mechanism of dye degradation in a photocatalytic dynamic membrane.

to C-O bond energy in the interface of CNG and zirconium dioxide [38,39]. Furthermore, the three peaks located at 398.85, 399.9, and 401 eV in the CNG-associated N 1s spectra are related to C=N-C, N-C_3, and N-H bonds, respectively. As can be seen, these peaks in CNGZ nanocomposite have a left-shift (398.6, 399.1, and 400.6 eV) compared to pure CNG, which illustrates that N atoms of CNG gain electrons from zirconium dioxide [38,39].

Effect of CNGZ nanocomposite dose

To examine the effect of the CNGZ nanocomposite dose on the dye photocatalytic degradation, 5, 15, and 30 mg of the nanocomposite were used for MB dye removal. Fig. 3 exhibits MB dye removal efficiency with various doses of CNGZ photocatalyst. Increasing the photocatalyst dose from 5 to 30 mg increases dye degradation efficiency, which can be attributed to greater access to surface adsorption sites and the creation of more electron-hole pairs that increase the degradation rate of pollutant molecules. Since the highest dye degradation efficiency was achieved with 30 mg of nanocomposite, this was selected as the optimal photocatalyst dose.

Self-Forming and pre-coated photocatalytic dynamic membrane

Fig. 4 shows MB and CR dye removal efficiency and rejection rate using batch processes and self-forming photocatalytic dynamic membranes, respectively. In both systems, the photocatalytic activity and removal of both dyes gradually increase. However, the self-forming dynamic membrane system has a greater degradation efficiency than the batch system. Note that the rejection rates of the pure PES membrane were respectively 29% and 47% for the MB and CR dyes. The results indicate that the highest rejection rate of MB and CR dyes corresponds to the self-forming system with the CNGZ nanocomposite at respectively 89% in 120 min and 100% in 80 min. The greater dye degradation rate of the CNGZ membrane relative to the CNG membrane can be attributed to the greater electron-hole pair separation rate and recombination prevention due to the zirconium dioxide presence in the nanocomposite sample. Zirconium dioxide traps the electrons transferred from the valence band to the conduction band of graphitic carbon nitride, preventing electron recombination. This produces more free radicals during photocatalysis, which, when contributing to the remaining pores in the valence band, degrade dye molecules (Scheme 2). Overall, the dye removal results point to the synergistic effect of the membrane process and photocatalysis, which improves the dynamic membrane's removal efficiency compared to the batch system (standalone photocatalysis).

As shown in Figs. 4 c and d, the self-forming dynamic membrane is more efficient and faster for removing CR dye than MB dye. Ultrafiltration membranes have wider pores than pollutant dye molecules and could let dye molecules through. Electrostatic repulsion between dye molecules and membrane surface somewhat compensates for the adverse effect of pore size and prevents dye molecules from passing. Given the anionic CR dye and the negatively-charged PES surface, the electrostatic repulsion between CR molecules

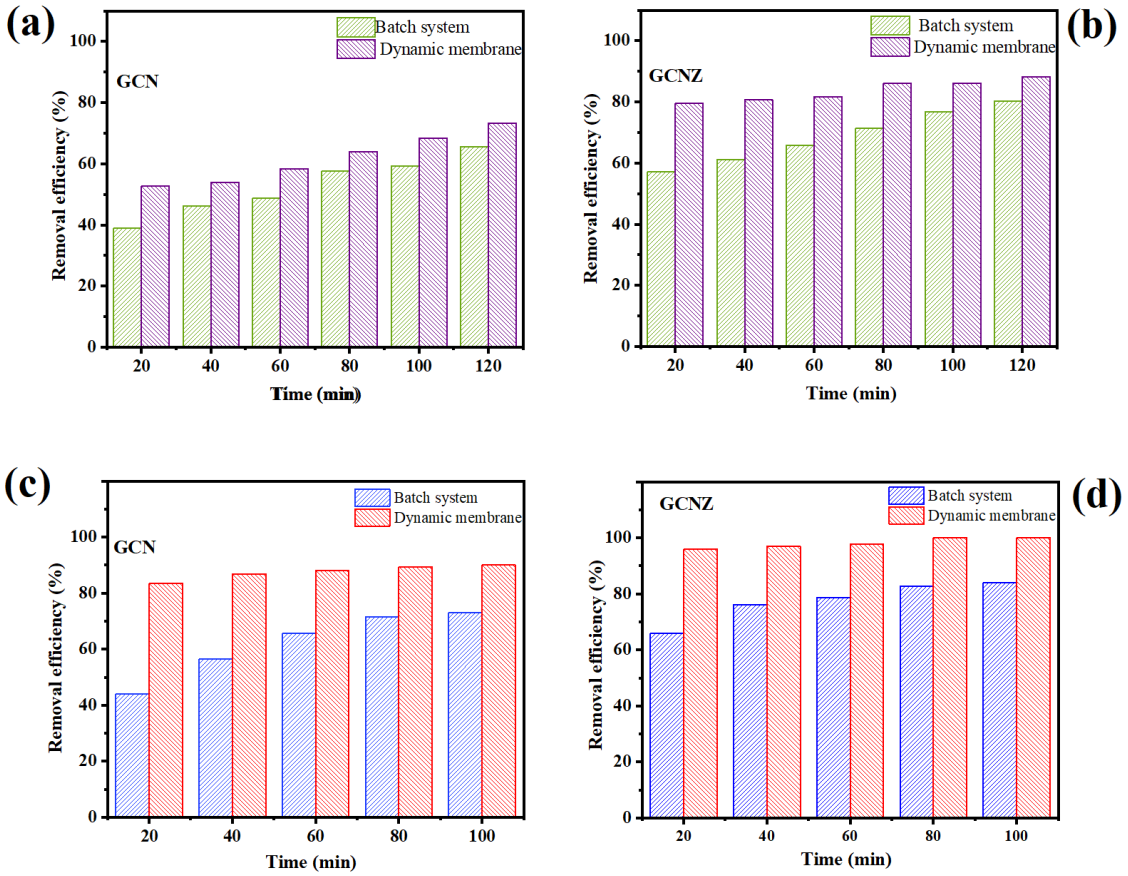

Fig. 4. Removal efficiency and rejection rate of (a,b) MB and (c,d) CR in the batch and self-forming membrane process (dye concentration: 10 mg/L).a

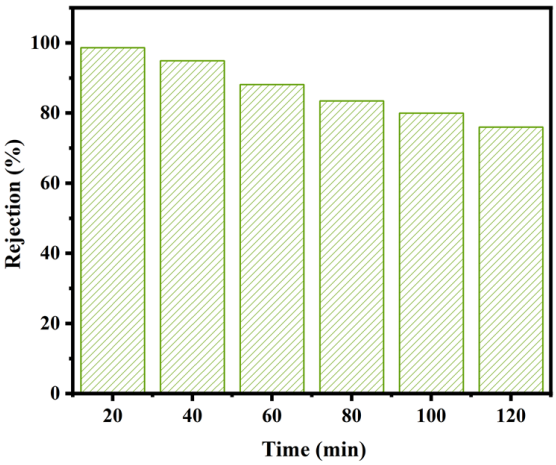

Fig. 5. Rejection rate of MB dye in the CNGZ pre-coated photocatalytic membrane (dye concentration: 10 mg/L).

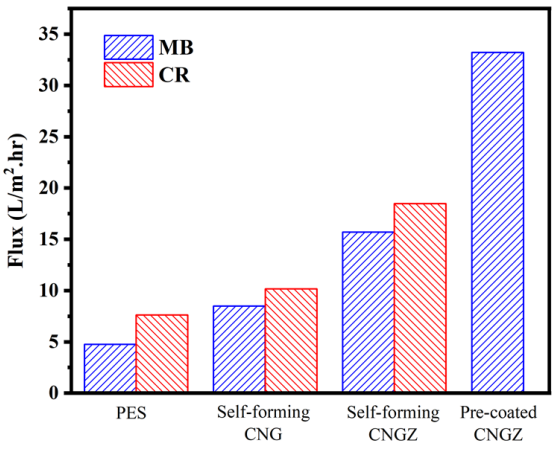

Fig. 6. Permeation flux of MB and CR in self-forming and pre-coated photocatalytic dynamic membrane (dye concentration: 10 mg/L).

and membrane surface blocks dye molecules from passing through the membrane, keeping dye molecules in the feed solution and degrading them by photocatalyst particles under light [12,40].

Fig. 5 shows the MB dye rejection rate of the CNGZ pre-coated photocatalytic dynamic membrane over time. In the first 20 min of filtration, the pre-coated membrane shows a high dye rejection rate of 98.6%. However, the value gradually decreases over time, which differs from the rejection rate changes of the self-forming membrane system. This can be attributed to the difference in the accessibility of photocatalyst particles to pollutant molecules in pre-coated and self-forming systems over time. The pre-coated system provides the highest dye removal efficiency at the beginning of filtration when most of the photocatalytic layer contacts a small number of dye molecules. The rejection ratio gradually decreases due to the reduction in untouched photocatalyst materials that contact pollutant molecules [2,41,42].

Fig. 6 shows the permeation flux of MB and CR dyes in the self-forming photocatalytic dynamic membrane. The pure PES membrane has the lowest permeation flux of 4.7 $\left(\frac{L}{m^2.hr}\right)$ for MB and 7.6 $\left(\frac{L}{m^2.hr}\right)$. for CR, which grows by adding the photocatalyst to the membrane system, which can be attrited to the high hydrophilicity of CNG and CNGZ photocatalysts.

The flux of the self-forming dynamic membrane containing CNGZ nanocomposite was obtained at 15.7 $\left(\frac{L}{m^2.hr}\right)$ and 18.5 $\left(\frac{L}{m^2.hr}\right)$ for MB and CR, respectively. Moreover, the dynamic membrane with the CNGZ nanocomposite achieves the highest flux due to the presence of hydrophilic zirconium dioxide nanosheets in the composite sample and its greater hydrophilicity than pure CNG [34].

Also, Fig. 6 shows that the pre-coated dynamic membrane containing the CNGZ photocatalyst achieves greater permeation flux for MB dye filtration than the self-forming dynamic membrane, which is in agreement with the results of several studies [2,43-46]. In the pre-coated membrane, the dynamic layer formed on the support membrane blocks dye molecules from passing through membrane pores. Before they reach the support membrane surface, the pollutant molecules are trapped by the upper photocatalytic layer and destroyed under light.

Kinetic Study

Based on zero-order, first-order, and second-order kinetic models, Figs. 7 and 8 show the fitness of experimental data for the batch system and the self-forming photocatalytic dynamic membrane for the MB and CR dyes. Moreover, Table 1 lists the kinetic parameters of mentioned models. As the table and the figures show, the experimental data of MB and CR removal using the batch system and the self-forming photocatalytic dynamic membrane follow the second-order model. Table 1 indicates that the highest constant rate for the MB and CR dyes corresponds to the self-forming photocatalytic dynamic membrane system with the CNGZ nanocomposite.

Comparison of the rejection efficiency with reported publications

The rejection efficiency of MB and CR dyes by various composite membranes is presented in Table 2. Compared with the listed membranes, the photocatalytic dynamic membrane constructed in this study illustrated good performance for both dyes.

CONCLUSION

In summary, the photocatalytic dynamic membrane was fabricated in self-forming and pre-coated modes with the CNGZ nanocomposite and used for removing organic pollutants from water under a household LED light. Both photocatalytic membrane systems showed exceptional dye degradation efficiency. Moreover, the dynamic membrane system outperformed standalone photocatalysis (batch system) in removing MB and CR dyes. The rejection rates of MB and CR dyes in the self-forming photocatalytic dynamic membrane with CNGZ were 89% in 120 min and 100% in 80 min, respectively. Furthermore, photocatalytic particles increased the permeation flux of the membrane system compared to the pure PES membrane. Moreover, the experimental data for the batch system and the self-forming dynamic membrane for both pollutant dyes were consistent with the second-order kinetic model. The results suggest that the self-forming photocatalytic dynamic membrane with the CNGZ nanocomposite is promising for increasing

Table 1. Parameters of zero, first, and second-order kinetic models for batch system and self-forming photocatalytic dynamic membrane (MB and CR concentration: 10 mg/L).

	Sample	Dye	Zero-order		First-order		Second-order	
			K_0	R^2	K_1	R^2	K_2	R^2
Batch system	CNG	MB	0.0307	0.9923	0.0056	0.9952	0.0011	0.9895
	CNGZ		0.0517	0.9382	0.0114	0.9775	0.0028	0.9918
Self-forming photocatalytic dynamic membrane	CNG	MB	0.0417	0.9469	0.0087	0.9777	0.0018	0.9873
	CNGZ		0.0671	0.8499	0.0187	0.8987	0.0065	0.9552
Batch system	CNG	CR	0.0404	0.9857	0.0091	0.9915	0.0022	0.9881
	CNGZ		0.0604	0.9128	0.0165	0.9559	0.0051	0.9887
Self-forming photocatalytic dynamic membrane	CNG	CR	0.0699	0.8507	0.0234	0.8914	0.0101	0.9435
	CNGZ		0.1309	0.8658	0.0679	0.9105	0.0791	0.9827

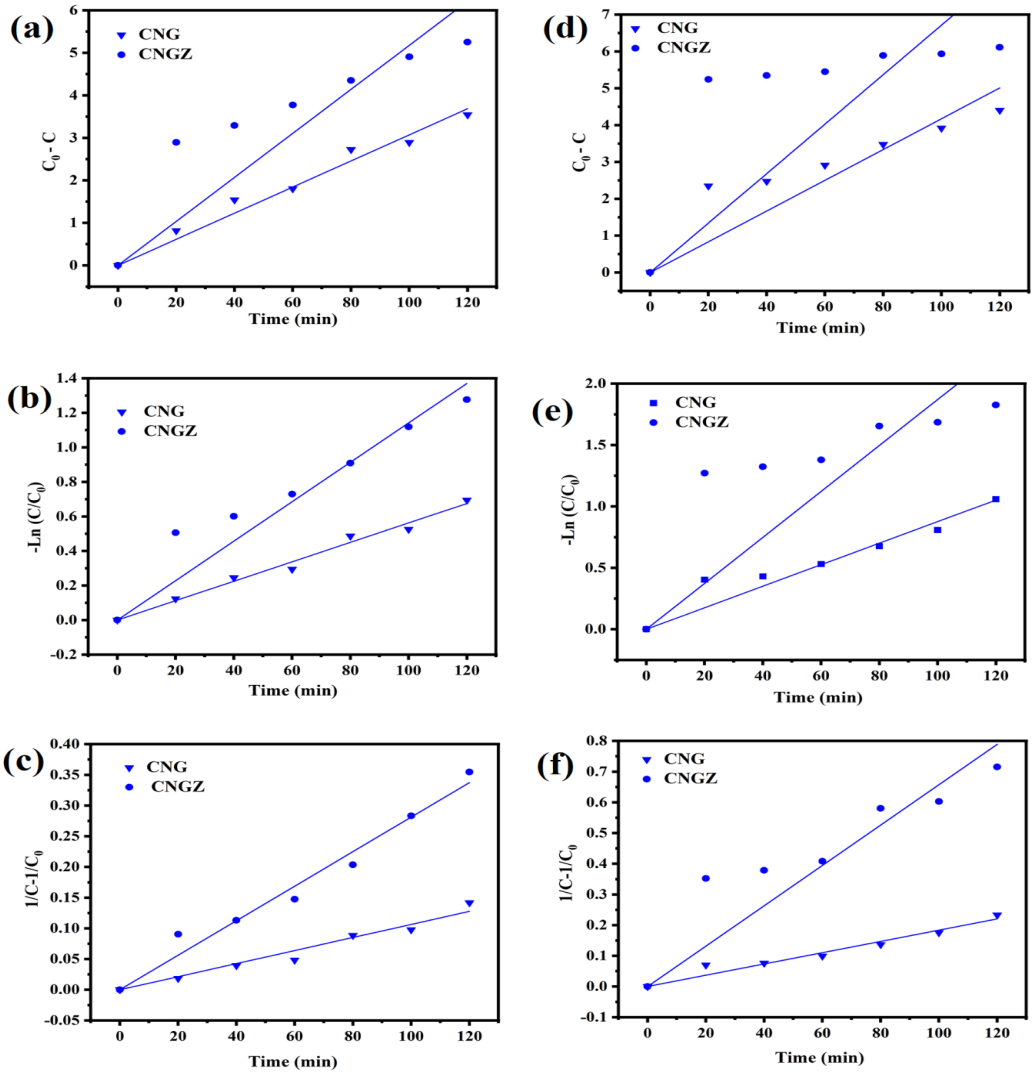

Fig. 7. Fitting the experimental data of MB removal with the zero-, first- and second-order models in (a-c) batch system and (d-f) self-forming photocatalytic dynamic membranes.

Table 2. Comparison of the rejection efficiency of MB and CR dyes by various membranes

membrane	Dye	Dye concentration (mg/L)	Rejection	Ref.
Chitosan/Organoclay/PVDF membrane	MB	1	80-95%	[47]
LA/Co^{2+}-ZnO@SSM composite membrane	MB	10	90%	[48]
PES/POM-TiO_2 mixed matrix membrane	MB	5	~73%	[49]
PVDF@rGO/TiO_2	MB	10	92%	[50]
PVDF@GO-MWCNTs/TiO_2			86.69%	
ZIF-67/PVDF membrane	CR	25	99.5%	[51]
ZIF-8/ Polyacrylonitrile composite membrane	CR	25	89%	[52]
MoS_2: PTCA/PES	CR	10	~80%	[53]
Photocatalytic dynamic membrane including	MB (self-forming)	10	89%	This Study
CNGZ nanocomposite	CR (self-forming)	10	100%	This Study
	MB (pre-coated)z	10	98.6%	This Study

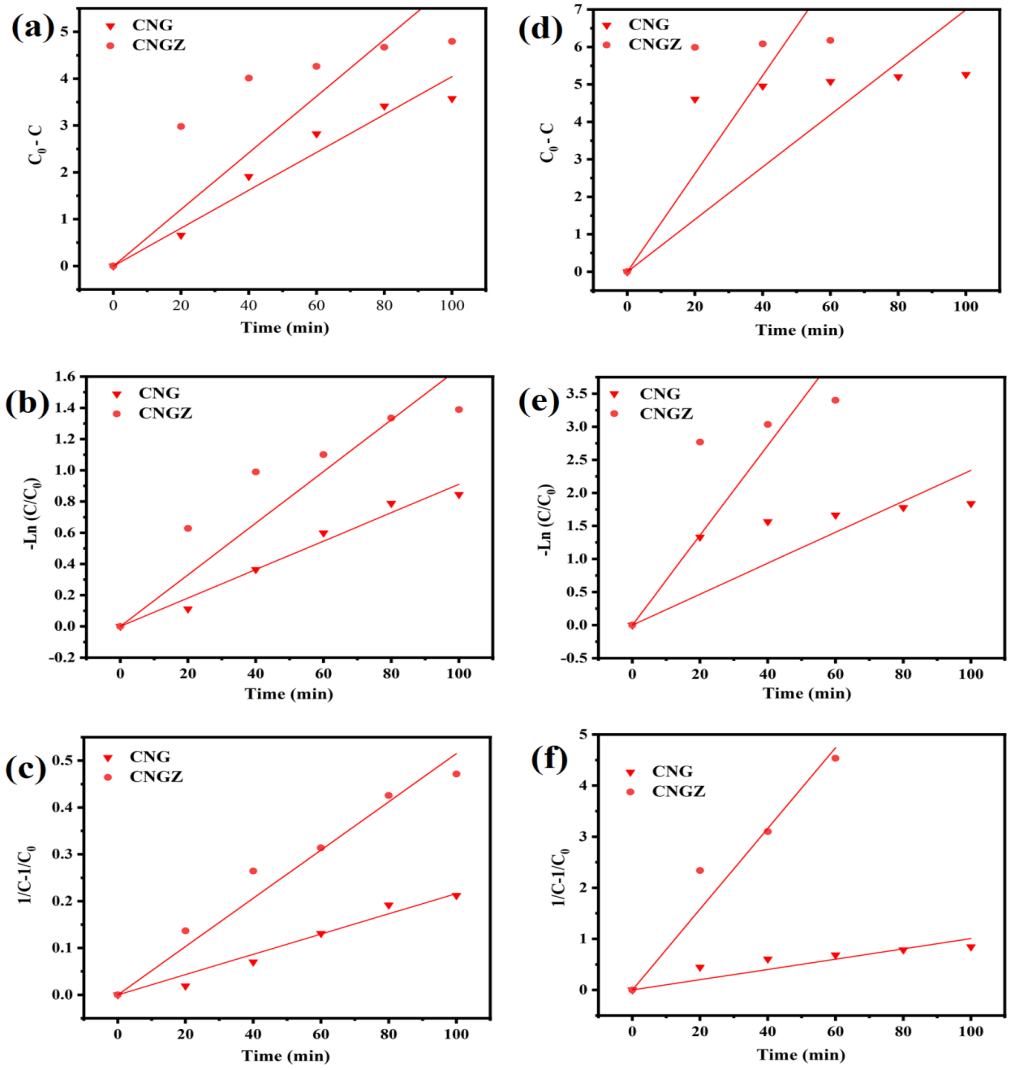

Fig. 8. Fitting the experimental data of CR removal with the zero-, first- and second-order models in (a-c) batch system and (d-f) self-forming photocatalytic dynamic membranes.

rejection rate and membrane flux in dye-containing wastewater treatment.

CONFLICT OF INTEREST

The authors hereby declare that there is no conflict of interest.

REFERENCES

1. L. Kaliraj, J.C. Ahn, E.J. Rupa, S. Abid, J. Lu, D.C. Yang, Synthesis of panosextract mediated ZnO nano-flowers as photocatalyst for industrial dye degradation by UV illumination, J. Photochem. Photobiol. B Biol. 199 2019, 111588. https://doi.org/10.1016/j.jphotobiol.2019.111588
2. Habibollahi, Z; Peyravi, M; Khalili, S; Jahnshahi, M. ZnO-based ternary nanocomposite for decolorization of methylene blue by photocatalytic dynamic membrane. Mater. Today Chem. 23, 2022, 100748. https://doi.org/10.1016/j.mtchem.2021.100748
3. Tahoura Saemian, Moayad Hossaini Sadr, Mohammad Tavakkoli Yaraki, Mehrnaz Gharagozlou, Behzad Soltani, Synthesis and characterization of CoFe2O4/SiO2/Cu-MOF for degradation of methylene blue through catalytic sono-Fenton-like reaction, Inorganic Chemistry Communications, 138, 2022, 109305. https://doi.org/10.1016/j.inoche.2022.109305
4. Robinson T., McMullan G., Marchant R., Nigam P., Remediation of dyes in textile effluent: a critical review on current treatment technologies with a proposed alternative, Bioresource technology, 77 (3), 2001, 247-255. https://doi.org/10.1016/S0960-8524(00)00080-8
5. Rafatullah M., Sulaiman O., Hashim R., Ahmad A., Adsorption of methylene blue on low-cost adsorbents: a review," Journal of hazardous materials, 177 (1-3), 2010, 70-80. https://doi.org/10.1016/j.jhazmat.2009.12.047
6. Salleh M. A. M., Mahmoud D. K., Karim W. A. W. A., Idris A., Cationic and anionic dye adsorption by agricultural solid wastes: a comprehensive review, Desalination, 280 (1-3), 2011, 1-13. https://doi.org/10.1016/j.desal.2011.07.019
7. Rauf M. A., Ashraf S. S., Survey of recent trends in biochemically assisted degradation of dyes, Chemical engineering journal, 209, 2012, 520-530. https://doi.org/10.1016/j.cej.2012.08.015
8. Gupta V., Suhas, Application of low-cost adsorbents for dye removal-a review, Journal of environmental management, 90 (8), 2009, 2313-2342. https://doi.org/10.1016/j.jenvman.2008.11.017
9. Dos Santos A. B., Cervantes F. J., Van Lier J. B., Review paper on current technologies for decolourisation of textile wastewaters: perspectives for anaerobic biotechnology, Bioresource technology, 98 (12), 2007, 2369-2385. https://doi.org/10.1016/j.biortech.2006.11.013
10. Cojocaru C., Clima L., Polymer assisted ultrafiltration of AO7 anionic dye from aqueous solutions: Experimental design, multivariate optimization, and molecular docking insights, Journal of Membrane Science, 604, 2020, 118054. https://doi.org/10.1016/j.memsci.2020.118054
11. Yang, C., Xu, W., Nan, Y., Wang, Y., Hu, Y., Gao, C., Chen, X., Fabrication and characterization of a high performance polyimide ultrafiltration membrane for dye removal. J. Colloid Interface Sci. 562, 2020, 589-597. https://doi.org/10.1016/j.jcis.2019.11.075
12. Jianhua Yun, Yixing Wang, Zhenying Liu, Yujie Li, Hu Yang, Zhen-liang Xu, High efficient dye removal with hydrolyzed ethanolamine-Polyacrylonitrile UF membrane: Rejection of anionic dye and selective adsorption of cationic dye, Chemosphere 259, 2020, 127390. https://doi.org/10.1016/j.chemosphere.2020.127390
13. Zhao H., Chen S., Quan X., Yu H., Zhao H., Integration of microfiltration and visible-light-driven photocatalysis on g-C3N4 nanosheet/reduced graphene oxide membrane for enhanced water treatment, Applied Catalysis B: Environmental, 194, 2016, 134-140. https://doi.org/10.1016/j.apcatb.2016.04.042
14. Wang L., Miao R., Wang X., Lv Y., Meng X., Yang Y., Huang D., Feng L., Liu Z., Ju K., Fouling behavior of typical organic foulants in polyvinylidene fluoride ultrafiltration membranes: characterization from microforces, Environmental Science & Technology, 47 (8), 2013, 3708-3714. https://doi.org/10.1021/es4004119
15. M. Kazemi, M. Peyravi, M. Jahanshahi, Multilayer UF membrane assisted by photocatalytic NZVI@TiO2 nanoparticle for removal and reduction of hexavalent chromium, J. Water Proc. Eng. 37, 2020, 101183. https://doi.org/10.1016/j.jwpe.2020.101183
16. S.F. Zakeritabar, M. Jahanshahi, M. Peyravi, J. Akhtari, Photocatalytic study of nanocomposite membrane modified by CeF3 catalyst for pharmaceutical wastewater treatment, J. Environ. Health Sci. and Eng. 18, 2020, 1151-1161. https://doi.org/10.1007/s40201-020-00534-4
17. M. Kazemi, M. Jahanshahi, M. Peyravi, Hexavalent chromium removal by multilayer membrane assisted by photocatalytic couple nanoparticle from both permeate and retentate, J. Hazard Mater. 344, 2018, 12-22. https://doi.org/10.1016/j.jhazmat.2017.09.059
18. Shokri, A., Using NiFe2O4 as a nano photocatalyst for degradation of polyvinyl alcohol in synthetic wastewater, Environmental Challenges, 5, 2021, 100332. https://doi.org/10.1016/j.envc.2021.100332
19. Shokri, A and Mahanpoor, K., Removal of Ortho-Toluidine from Industrial Wastewater by UV/TiO2 Process, Journal of chemical health risks, 6(3), 2016, 213-223.
20. Shokri, A., Salimi. M., Abmatin, T., Employing photo Fenton and UV/ZnO processes for removing Reactive red 195 from aqueous environment, Fresenius Environmental Bulletin, 26(2-A), 1560-1565.
21. Saghi, M., Shokri, A., Arastehnodeh, A., Khazaeinejad, M., Nozari, A., The photo degradation of methyl red in aqueous solutions by α-Fe2O3/SiO2 nano photocatalyst, J. Nanoanalysis., 5(3), 2018, 163-170.
22. Liu T., Wang L., Liu X., Sun C., Lv Y., Miao R., Wang X., Dynamic photocatalytic membrane coated with ZnIn2S4 for enhanced photocatalytic performance and antifouling property, Chemical Engineering Journal, 379, 2020, 122379. https://doi.org/10.1016/j.cej.2019.122379
23. Ding, C.H., Qin, X., Tian, Y., Cheng, B., PES membrane surface modification via layer-by-layer self-assembly of GO@TiO2 for improved photocatalytic performance, Journal of Membrane Science, 659, 2022, 120789. https://doi.org/10.1016/j.memsci.2022.120789
24. Abbas Ahmadi, Mohammad Hossein Sarrafzadeh, Maryam Mohamadi, Zeinab Mahdigholian, Akram Hosseinian, Investigation on polysulfone blended NH2-MIL125 (Ti) membrane for photocatalytic degradation of Methylene Blue

dye, Journal of water and environmental nanotechnology, 5 (3), 2020, 234-245.
25. Yu L., Han M. and He F., A review of treating oily wastewater, Arabian Journal of Chemistry, 2017, 1913-1922. https://doi.org/10.1016/j.arabjc.2013.07.020
26. Bo Gao, Weiping Chen, Jiadong Liu, Jiajun An, Lei Wang, Ying Zhu, Mika Sillanp¨a¨a, Continuous removal of tetracycline in a photocatalytic membrane reactor (PMR) with ZnIn2S4 as adsorption and photocatalytic coating layer on PVDF membrane, Journal of Photochemistry and Photobiology A: Chemistry, 364, 2018, 732-739. https://doi.org/10.1016/j.jphotochem.2018.07.008
27. Y.M. Yu, J.F. Geng, H. Li, R.Y. Bao, H.Y. Chen, W.Z. Wang, J.X. Xia, W.Y. Wong, Exceedingly high photocatalytic activity of g-C3N4/Gd-N-TiO2 composite with nanoscale heterojunctions, Sol. Energ. Mat. Sol. C. 168, 2017, 91-99. https://doi.org/10.1016/j.solmat.2017.04.023
28. Yeganeh Kosar Hashemi, Mohammad Tavakkoli Yaraki, Sina Ghanbari, Leily Heidarpoor Saremi, Mohammad Hadi Givianrad, Photodegradation of organic water pollutants under visible light using anatase F, N co-doped TiO2/SiO2 nanocomposite: Semi-pilot plant experiment and density functional theory calculations, Chemosphere, 275, 2021, 129903. https://doi.org/10.1016/j.chemosphere.2021.129903
29. Mahdieh Chegeni, Mozhgan Mehri, Mehdi Hosseini, The MoS2/S-doped graphitic carbon nitride: synthesis and application as a composite for removing organic pollutant, Journal of water and environmental nanotechnology, 5 (4), 2020,331-341. https://doi.org/10.1002/slct.201903885
30. Ghader Hosseinzadeh, Innovative synthesis of TiO2 nanorod/WO3 nanoflakes heterojunction photocatalyst for visible light degradation of Nitenpyram insecticide, Journal of water and environmental nanotechnology, 7 (3), 2022, 230-240.
31. Emelda Rayappan, Jayarajan Muthaian, Muthirulan Pandi, Investigation on the photocatalytic activity of chemically synthesized zirconium doped cadmium selenide nanoparticles for indigo carmine dye degradation under solar light irradiation, 6 (2), 2021, 177-187.
32. VP Letswalo, LN Dlamini, SP Malinga, Efficient degradation of tetracycline using a nanostructured g-C3N4/Nb2O5/HPEI/PES photocatalytic membrane, Environmental Advances 10, 2022, 100322. https://doi.org/10.1016/j.envadv.2022.100322
33. Shuo Shi, Mingmin Jia, Meisheng Li, Shouyong Zhou, Yijiang Zhao, Jing Zhong, Dingliang Dai, Jianhao Qiu, ZnO@g-C3N4 S-scheme photocatalytic membrane with visible-light response and enhanced water treatment performance, Colloids and Surfaces A: Physicochemical and Engineering Aspects 667, 2023, 131259. https://doi.org/10.1016/j.colsurfa.2023.131259
34. Marjan Tanzifi, Mohsen Jahanshahi, Majid Peyravi, Soodabeh Khalili, A morphological decoration of g-C3N4/ZrO2 heterojunctions as a visible light activated photocatalyst for degradation of various organic pollutants, Journal of Environmental Chemical Engineering, 10, 2022, 108600. https://doi.org/10.1016/j.jece.2022.108600
35. Ahmad Jonidi-Jafari, Mehdi Shirzad-Siboni, Jae-Kyu Yang, Mohammad Naimi-Joubani, Mehrdad Farrokhi, Photocatalytic degradation of diazinon with illuminated ZnO-TiO2 composite, Journal of the Taiwan Institute of Chemical Engineers, 50, 2015, 100-107. https://doi.org/10.1016/j.jtice.2014.12.020
36. Xin Zhang, Xingzhong Yuan, Longbo Jiang, Jin Zhang, Hanbo Yu, Hou Wang, Guangming Zeng, Powerful combination of 2D g-C3N4 and 2D nanomaterials for photocatalysis: Recent advances, Chemical Engineering Journal, 390, 2020, 124475. https://doi.org/10.1016/j.cej.2020.124475
37. Qingling Chen, Wulin Yang, Jiajun Zhu, Licai Fu, Deyi Li, Lingping Zhou, Enhanced visible light photocatalytic activity of g-C3N4 decorated ZrO2-x nanotubes heterostructure for degradation of tetracycline hydrochloride, Journal of Hazardous Materials 384, 2020, 121275. https://doi.org/10.1016/j.jhazmat.2019.121275
38. Huanhuan Li, Yong Wu, Can Li, Yinyan Gong, Lengyuan Niu, Xinjuan Liu, Qing Jiang, Changqing Sun, Shiqing Xu, Design of Pt/t-ZrO2/g-C3N4 efficient photocatalyst for the hydrogen evolution reaction, Applied Catalysis B: Environmental 251, 2019, 305-312. https://doi.org/10.1016/j.apcatb.2019.03.079
39. Muyan Zhou, Yong Wu, Lingyi Shi, Shiyu Hu, Huanhuan Li, Yinyan Gong, Lengyuan Niu, Xinjuan Liu, Can Li, Excellent Photocatalytic Efficiency of t-ZrO2/g-C3N4 Photocatalyst for Pollutants Degradation: Experiment and theory, Solid State Sciences 104, 2020, 106202. https://doi.org/10.1016/j.solidstatesciences.2020.106202
40. Yehia Manawi, Viktor Kochkodan, Ebrahim Mahmoudi, Daniel J. Johnson, Abdul Wahab Mohammad and Muataz Ali Atieh, Characterization and Separation Performance of a Novel Polyethersulfone Membrane Blended with Acacia Gum, Scientific Reports, 7 (15831), 2017. https://doi.org/10.1038/s41598-017-14735-9
41. F. Doagoo, M. Peyravi, S. Khalili, Photo-degradation and discoloration of nitrogen substituted ZnO via multilayer adsorptive membrane for Cr (VI) removal, J. Environ. Chem. Eng. 9, 2021, 105153. https://doi.org/10.1016/j.jece.2021.105153
42. Y. Bao, X. Yan, W. Du, X. Xie, Z. Pan, J. Zhou, L. Li, Application of aminefunctionalized MCM-41 modified ultrafiltration membrane to remove chromium (VI) and copper (II), Chem. Eng. J. 281, 2015, 460-467. https://doi.org/10.1016/j.cej.2015.06.094
43. M. Peyravi, M. Jahanshahi, S.M. Mirmousaei, W.-J. Lau, Dynamically coated photocatalytic zeolite-TiO2 membrane for oil-in-water emulsion separation, Arabian J. Sci. Eng., 46, 2020, 6143-6151. https://doi.org/10.1007/s13369-019-04335-2
44. S. Mirmousaei, M. Peyravi, M. Khajouei, M. Jahanshahi, S. Khalili, Preparation and characterization of nano-filtration and its photocatalytic abilities via pre-coated and self-forming dynamic membranes developed by ZnO, PAC and chitosan, Water Sci. Technol., 80, 2019, 2273-2283. https://doi.org/10.2166/wst.2020.044
45. M. Darzipour, M. Jahanshahi, M. Peyravi, S. Khalili, Antibacterial dynamic membranes loaded by cephalexin/amine-functionalized SBA_15 for Pb (II) ions removal, Kor. J. Chem. Eng., 36 2019, 2035-2046. https://doi.org/10.1007/s11814-019-0391-y
46. N.G. Chepi, M. Peyravi, M. Jahanshahi, Ultrafiltration of O/W emulsion by dynamic polyester support: a comparison study between self-forming and pre-coated, Chem. Pap., 74, 2020, 2111-2122. https://doi.org/10.1007/s11696-020-01059-8
47. P. Daraei, S.S. Madaeni, E. Salehi, N. Ghaemi, H.S. Ghari, M.A.

Khadivi, E. Rostami, Novel thin film composite membrane fabricated by mixed matrix nanoclay/chitosan on PVDF microfiltration support: preparation, characterization and performance in dye removal. J. Membr. Sci. 436, 2013, 97-108. https://doi.org/10.1016/j.memsci.2013.02.031

48. Q. Wu, W. Zhang, C.H. Qu, F. Yuan, Y. Huang, X. Chen, R. Zhang, Lauric acid surface modified Co2+-ZnO@SSM composite membrane: Photocatalytic degradation of MB and oil/water separation for removal of organic pollutants, Applied Surface Science, 622, 2023, 156933. https://doi.org/10.1016/j.apsusc.2023.156933
49. S. Zhafiri, B. Tamam Ibnu Ali, T. Gunawan, N. Widiastuti, Fabrication of PES/POM-TiO2 mixed matrix membrane with photocatalytic activity for methylene blue removal, Materials Today: Proceedings, 74, 2023, 471-475. https://doi.org/10.1016/j.matpr.2022.11.256
50. R. Mohamat, S. Abu Bakar, A. Mohamed, Muqoyyanah, S. Nur Elida Aqmar Mohamad Kamal, M.H. Dzarfan Othman, R. Rohani, M.H. Mamat, M.F. Malek, M. Khairul Ahmad, S. Ramakrishna, Methylene blue rejection and antifouling properties of different carbonaceous additives-based polyvinylidene fluoride membrane, Materials Today Communications, 35, 2023, 105862. https://doi.org/10.1016/j.mtcomm.2023.105862
51. U. Sharma, R. Pandey, S. Basu, P. Saravanan, ZIF-67 blended PVDF membrane for improved Congo red removal and antifouling properties: A correlation establishment between morphological features and ultrafiltration parameters, Chemosphere, 320, 2023, 138075. https://doi.org/10.1016/j.chemosphere.2023.138075
52. M. Li, J. Luo, J. Lu, W. Shang, J. Mu, F. Sun, Z. Dong, X. Li, A novel nanofibrous PAN ultrafiltration membrane embedded with ZIF-8 nanoparticles for effective removal of Congo red, Pb(II), and Cu(II) in industrial wastewater treatment, Chemosphere, 304, 2022, 135285. https://doi.org/10.1016/j.chemosphere.2022.135285
53. M. Sreeramareddygari, J. Mannekote Shivanna, M. Somasundrum, K.H. Soontarapa, W. Surareungchai, Polythiocyanuric acid-functionalized MoS2 nanosheet-based high flux membranes for removal of toxic heavy metal ions and congo red, Chemical Engineering Journal, 425, 2021, 130592. https://doi.org/10.1016/j.cej.2021.130592